BG

GSI

STUDY OF THE OUT-OF-PLANE EMISSION OF PROTONS AND LIGHT FRAGMENTS IN SYMMETRIC HEAVY-ION COLLISIONS

D. BRILL, P. BECKERLE, C. BORMANN, E. SCHWAB, Y. SHIN, R. STOCK,
H. STRÖBELE, P. BALTES, C. MÜNTZ, H. OESCHLER, C. STURM, A. WAGNER,
R. BARTH, M. CIESLAK, M. DEBOWSKI, E. GROSSE, P. KOCZON, M. MANG,
D. MISKOWIEC, R. SCHICKER, P. SENGER, B. KOHLMEYER, F. PÜHLHOFER,
J. SPEER, K. VÖLKEL, W. WALUS

sw9606

Study of the Out-of-Plane Emission of Protons and Light Fragments in Symmetric Heavy-Ion Collisions

D. Brill[1], P. Beckerle[1], C. Bormann[1], E. Schwab[1], Y. Shin[1], R. Stock[1], H. Ströbele[1], P. Baltes[2], C. Müntz[2*], H. Oeschler[2], C. Sturm[2], A. Wagner[2], R. Barth[3], M. Cieślak[3], M. Dębowski[3], E. Grosse[3], P. Koczoń[3], M. Mang[3], D. Miśkowiec[3**], R. Schicker[3], P. Senger[3], B. Kohlmeyer[4], F. Pühlhofer[4], J. Speer[4], K. Völkel[4], and W. Waluś[5]

[1] Johann Wolfgang Goethe-Universität, D-60325 Frankfurt/Main, Germany
[2] Technische Hochschule Darmstadt, D-64289 Darmstadt, Germany
[3] Gesellschaft für Schwerionenforschung, D-64220 Darmstadt, Germany
[4] Philipps-Universität, D-35037 Marburg, Germany
[5] Jagiellonian University, PL-30-059 Kraków, Poland

December 22, 1995

Abstract. Midrapidity protons from $^{209}Bi + ^{209}Bi$ collisions were measured with the Kaon Spectrometer at SIS at incident energies of $E_{Lab}/A = 400, 700$ and 1000 MeV. Additionally, light fragments were analysed at 400 MeV. We have investigated the azimuthal emission pattern of the particles relative to the reaction plane as function of transverse momentum, bombarding energy and impact parameter. We observe an enhanced emission of particles perpendicular to the reaction plane at all bombarding energies. The ratio of the number of particles emitted out-of-plane/in-plane increases strongly with the particles transverse momentum. The anisotropy decreases with increasing beam energy. Composite particles show a much stronger effect than protons

PACS: 25.75.+r

1. Introduction

Collective flow effects are - besides particle production - the most important tool to investigate hot and compressed nuclear matter produced in relativistic nucleus-nucleus collisions [1, 2, 3]. Pioneering experiments have established two kinds of collective effects from the overlap region between two colliding nuclei: The directed flow of nucleons in the reaction plane ("side splash") and the preferred emission of nucleons perpendicular to the reaction plane ("squeeze-out")[4-10]. In particular, the latter is a very promising tool to extract information about the dynamics of hot and compressed nuclear matter. A collective out-of-plane emission was predicted by early hydrodynamical calculations and interpreted as a dynamical squeeze out of matter due to the build-up of pressure in the interaction zone of the two colliding nuclei [11]. Further theoretical studies in the framework of microscopic models (QMD) found a strong sensitivity to the nuclear equation of state (EOS) for this effect [12].

According to microscopic models [13] many of the observables in heavy-ion reactions are sensitive to both: the EOS and momentum-dependent interactions (MDI).

However, in contrast to flow effects in the reaction plane, the particle flow out-of-plane is expected to be less sensitive to momentum-dependent interactions [14].

Previous experimental results are in qualitative agreement with model calculations. However, quantitative comparisons are difficult since these data are subject to acceptance cuts as well as basic experimental uncertainties in determining the reaction geometry. Therefore, we have analysed the strength of the out-of-plane emission of particles corrected for the uncertainty in determining the reaction plane as a function of transverse momentum. We expect that quantitative comparisons of model calculations with our experimental data will lead to an improved determination of the EOS.

2.1 Experimental Setup

The experiment was performed with the Kaon Spectrometer at the Darmstadt (GSI) heavy ion synchrotron SIS [15]. This spectrometer is a double-focussing QD configuration with large solid angle (15-30 msr) and wide momentum acceptance. Particle identification is obtained by measuring momentum and velocity. The momentum is determined from the focal-plane position of the particle trajectories, whereas the velocity is calculated by using information on time-of-flight. Two scintillator detector arrays added to the spectrometer provide additional information to characterize the event [15-18]. The Large Angle Hodoscope gives information on the charged particle multiplicity which is a measure of the impact parameter. This detector consists of 96 modules and accepts charged particles in the polar angular range $12° < \Theta_{Lab} < 48°$. Particles emitted into this angular range are predominantly participating protons. The second external detector, the Small Angle Hodoscope, is located 7 meters downstream of the target. This array is composed of 380 modules and covers polar angles $0.5° < \Theta_{Lab} < 7°$. Most of the particles emitted in this angular range are projectile spectator nucleons. This detector system provides information on polar angle, azimuth, charge and time-of-flight. Projectile spectators are identified by the ΔE signal in the scintillator modules and by time-of-flight. The azimuth of the iden-

---

* Present address: BNL, Upton, NY 11973, USA
** Present address: SUNY, Stony Brook, NY 11794-3800, USA

tified spectators is used to reconstruct the event plane. We used ^{209}Bi projectiles of $E_{Lab}/A = 400, 700$ and 1000 MeV with a beam intensity of 10^5 particles per spill and Bi-targets with a thickness of 0.92 g/cm^2 and 0.35 g/cm^2. Figure 1 shows the energy-loss in one of the scintillator paddles of the time-of-flight detector in the focal-plane versus the mass/Z-ratio of particles detected in the spectrometer. The measurements were done at different magnetic field settings corresponding to the different momentum ranges. The polar angle of the spectrometer was varied to select particle rapidities in the range of $0.35 < y/y_{proj} < 0.65$
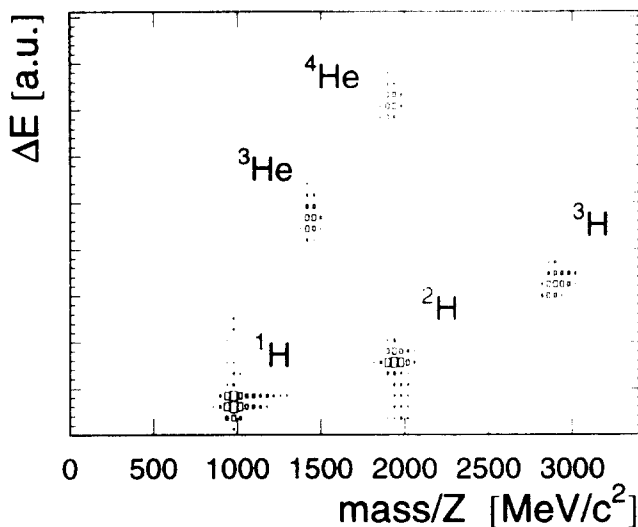

Fig. 1. Energy-loss in one scintillator paddle of the time-of-flight detector versus the mass/Z-ratio of particles in the spectrometer

2.2 Impact Parameter Determination

Following the method devised previously [7] we have divided the multiplicity distribution measured with the Large Angle Hodoscope into five groups (MUL1 to MUL5) to classify the reaction centrality. MUL1(MUL5) indicates the lowest(highest) multiplicity bin corresponding to peripheral(central) collisions. The measured hit multiplicity of charged particles for each multiplicity bin is given in Tab. 1.

E_{Lab}/A	MUL1	MUL2	MUL3	MUL4	MUL5
400 MeV	< 15	15 - 28	29 - 41	42 - 55	> 55
700 MeV	< 16	16 - 31	32 - 47	48 - 62	> 62
1000 MeV	< 17	17 - 33	34 - 49	50 - 65	> 65

Table 1. Hit multiplicity range of charged particles measured with the Large Angle Hodoscope in each multiplicity bin used for the impact parameter selection. Note that no multiple hit correction has been applied.

Assuming the clean-cut geometrical model [19] the number of participants is a monotonously decreasing function of the impact parameter b. The Large Angle Hodoscope covers a wide range of the participant's phase space and therefore the number of participants can be deduced from the measured hit multiplicity of this detector.

For each multiplicity range, MUL1 to MUL5, the number of participating protons Z_{part} and the corresponding impact parameters <b> are extracted from a simulation which includes the detector geometry of the Large Angle

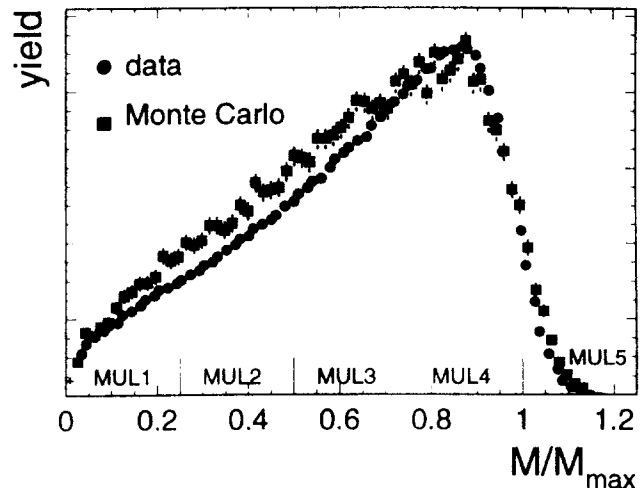**Fig. 2.** Normalized multiplicity distribution of charged particles as measured with the Large Angle Hodoscope at $E_{Lab}/A = 400$ ($M_{max} = 55$) and the corresponding values as determined by the simulation. The ordinate is linear starting at zero. Note that the shape of the distribution is biased by the spectrometer trigger.

Hodoscope. An event generator based on the clean-cut model yields a number of charged participants Z_{part} and pions, respectively, for a given impact parameter b. The participating nucleons emitted as Z=1 and Z=2 particles are assumed to have a Maxwell-Boltzmann momentum distribution in the center of mass system. The particle ratios He/H are extracted from the spectrometer data [20]. The momenta are boosted into the laboratory frame according to the incident energy. The calculated

E_{Lab}/A	MUL1	MUL2	MUL3	MUL4	MUL5
400 MeV	10.9 fm	8.7 fm	6.2 fm	3.4 fm	1.6 fm
700 MeV	10.8 fm	8.6 fm	6.3 fm	3.6 fm	1.6 fm
1000 MeV	11.0 fm	9.0 fm	6.7 fm	3.9 fm	1.7 fm

Table 2. The average impact parameters <b> estimated from the measured hit multiplicity of charged particles in each multiplicity bin. Errors on <b> are estimated to be smaller than ±0.3 fm (see text).

hit-multiplicity patterns in the Large Angle Hodoscope reproduce very well the shape of the measured ones. This is shown in Fig. 2 for $E_{Lab}/A = 400$ MeV. However, the measured hit multiplicities at $E_{Lab}/A = 700$ MeV and 1000 MeV are 20% and 30%, respectively, higher than the simulated ones. This can be explained by additional hits in the detector caused by photons from neutral pions or secondary reaction products. The measured average hit multiplicities increase with increasing beam energies as shown in Tab. 1. From the simulated multiplicity pattern we extracted the corresponding impact parameter distributions. Table 2 shows the average impact parameter <b> of the distributions for the multiplicity ranges MUL1 to MUL5. The extracted widths of

the distributions are approximately $\sigma \approx 1$ fm. The systematic errors due to particle ratio uncertainties are estimated to be smaller than ± 0.3 fm. The values of $<b>$ are in good agreement with previous results which were obtained by measuring the charged projectile spectators of $^{197}Au+^{197}Au$ collisions at $E_{Lab}/A = 1000$ MeV [21].

2.3 Reaction Plane Determination

For the reconstruction of the event plane the transverse momentum method is used [22]. This method yields a reaction plane for each event defined by the beam axis and a vector Q, which is the vector sum of the transverse momenta of all spectator particles observed in the Small Angle Hodoscope [17, 21]. The event plane is characterized by the azimuth Φ. The experimental uncertainty of

E_{Lab}/A	400 MeV	700 MeV	1000 MeV
MUL1	10.2 (5.3)	18.7 (8.1)	23.7 (10.7)
MUL2	13.9 (3.7)	21.2 (4.4)	26.3 (5.5)
MUL3	11.1 (3.4)	16.8 (4.2)	21.8 (4.9)
MUL4	5.9 (3.0)	9.6 (3.9)	13.0 (4.8)
MUL5	3.7 (2.2)	6.2 (2.7)	8.8 (3.7)

Table 3. Measured average multiplicity per event of charged particles in the Small Angle Hodoscope used for the reaction plane reconstruction. The values are given for different beam energies and multiplicity ranges. The widths σ of the corresponding multiplicity distributions are given in brackets.

the event plane reconstruction is estimated by randomly subdividing each event into two subevents, each containing one half of all particles [22]. For each subevent one evaluates the independent vectors Q_i $(i=1,2)$ and extracts the angle $\Delta\Phi_{12}=\Phi_1-\Phi_2$ between the two vectors. From the probability distribution $P(|\Delta\Phi_{12}|)$ one can estimate the uncertainty in determining the reaction plane for the complete event.

The procedure is done in two steps. First, the experimental distribution $P(|\Delta\Phi_{12}|)$ is used to estimate the accuracy of the angle $\Delta\Phi_{12}$ between two subevents. In a second step the probability distribution $P(|\Delta\Phi_{12}|)$ is reproduced by a Monte Carlo simulation in which the true reaction plane is known and the probability distribution $P(|\Delta\Phi|)$ between the true and the reconstructed reaction plane is calculated. From this distribution the difference between the true and the reconstructed reaction plane $\Delta\Phi=\Phi_{true}-\Phi_{est}$ is estimated. The Monte Carlo procedure takes the detector geometry of the Small Angle Hodoscope into account and simulates a projectile spectator source. The generated event multiplicities as well as the momenta of the particles have been adjusted to reproduce the hit multiplicities (shown in Tab. 3) and transverse momenta of the spectators measured with the Small Angle Hodoscope. The spectator momenta have been generated with a Gaussian momentum distribution. The deflection into the reaction plane is simulated by an additional transverse momentum kick for each particle parallel to the vector Q.
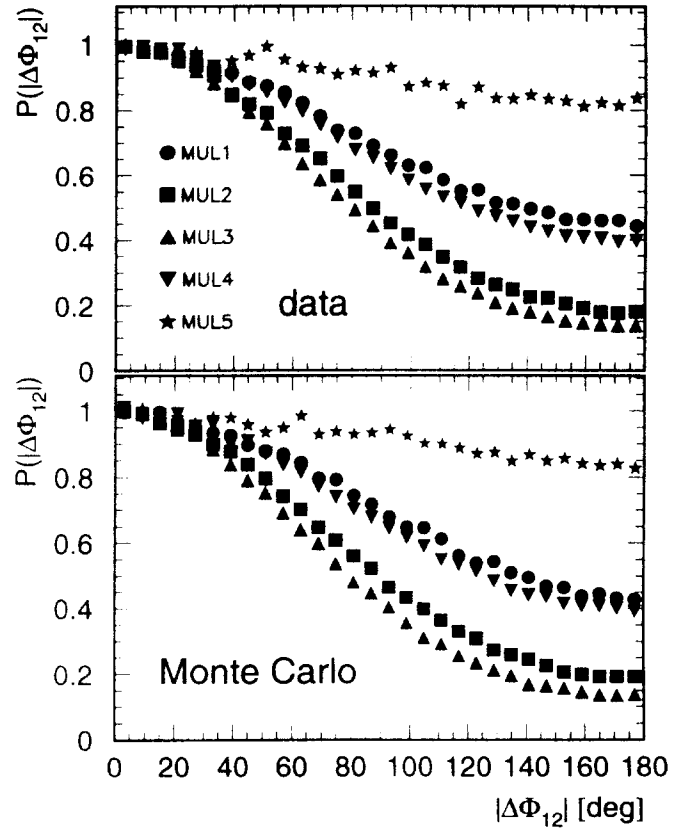

Fig. 3. Probability distribution $P(\Delta\Phi_{12})$ for the angular difference $\Delta\Phi_{12}$ between Q_1 and Q_2 as measured at a beam energy of $E_{Lab}/A = 1000$ MeV (upper) and simulated (lower). The distributions are shown for different multiplicity ranges.

$E_{Lab}/A = 400$ MeV		
	$< \Delta\Phi_{12}^2 >^{1/2}$	$< \Delta\Phi^2 >^{1/2}$	$< cos(2\Delta\Phi) >$
MUL1	98.2°	74.3°	0.13
MUL2	86.4°	51.9°	0.35
MUL3	82.1°	47.4°	0.41
MUL4	93.5°	67.4°	0.18
MUL5	100.5°	86.5°	0.03

$E_{Lab}/A = 700$ MeV		
	$< \Delta\Phi_{12}^2 >^{1/2}$	$< \Delta\Phi^2 >^{1/2}$	$< cos(2\Delta\Phi) >$
MUL1	91.7°	59.5°	0.27
MUL2	76.7°	40.2°	0.49
MUL3	75.0°	39.7°	0.51
MUL4	91.7°	61.0°	0.25
MUL5	101.2°	85.8°	0.04

$E_{Lab}/A = 1000$ MeV		
	$< \Delta\Phi_{12}^2 >^{1/2}$	$< \Delta\Phi^2 >^{1/2}$	$< cos(2\Delta\Phi) >$
MUL1	91.7°	54.9°	0.30
MUL2	77.5°	40.0°	0.50
MUL3	73.1°	36.4°	0.55
MUL4	89.0°	55.9°	0.31
MUL5	101.1°	80.5°	0.08

Table 4. Uncertainties of the azimuthal difference between the reaction plane calculated from the subevents and between the estimated and the true reaction plane, respectively, as extracted from the simulation (see text). The statistical errors are negligible.

The upper picture in Fig. 3 shows the measured probability distribution $P(|\Delta\Phi_{12}|)$ between Q_1 and Q_2 extracted from the data at a beam energy of $E_{Lab}/A = 1000$ MeV. The lower picture shows the corresponding distribution obtained by the Monte Carlo simulation. The results of the Monte Carlo simulation, given in Tab. 4, show the dispersions $< \Delta\Phi_{12}^2 >^{1/2}$ and $< \Delta\Phi^2 >^{1/2}$ of the azimuthal difference $\Delta\Phi_{12}$ and $\Delta\Phi$, respectively. If there is no correlation between the two vectors the values for $< \Delta\Phi_{12}^2 >^{1/2}$ and $< \Delta\Phi^2 >^{1/2}$ are about $104°$ degrees. The values of $< \Delta\Phi^2 >^{1/2}$ are lower than the values of $< \Delta\Phi_{12}^2 >^{1/2}$. This improvement in accuracy arises from a doubling of the multiplicity and the change from a deviation between two found vectors to a deviation from one found vector Q [22].

3. Results

We first demonstrate the azimuthal asymmetry of the observed emission pattern. Figure 4 shows the azimuthal distribution of the vector Q around the beam axis for events for which H-isotopes are observed in the spectrometer. The angle φ is the relative azimuthal angle between the estimated reaction plane and the emitted particle. The distributions show maxima around $\pm 90°$ with respect to the event plane. This pattern demonstrates the preferred emission of particles out of the reaction plane. The distributions are parametrized by the expression $N(\varphi) \sim 1 + P_1 \cos(\varphi) + P_2 \cos(2\varphi)$.

The parameter P_1 is related to the in-plane emission of the particles and is zero for particles emitted around midrapidity. The spectrometer acceptance for different particles is not symmetric with respect to midrapidity. In our case the measured protons and deuterons stem predominantly from the forward hemisphere whereas most tritons have backwards rapidities. This results in values of P_1 different from zero (^{1}H: $P_1 = 0.04$, ^{2}H: $P_1 = 0.03$, ^{3}H: $P_1 = -0.27$).

Negative values of P_2 indicate an out-of-plane emission. In Tab. 5 the parameters P_2 for protons are given for the multiplicity bins MUL1 to MUL4 and different transverse-momentum ranges.

The values P_2 are affected by the uncertainty in determining the reaction plane. The true values P_2' are larger than the measured P_2. Therefore, the P_2 coefficients have been corrected for the fluctuations $\Delta\Phi$ of the estimated reaction plane with respect to the true reaction plane by the relation [5]: $P_2' = P_2/< cos(2\Delta\Phi) >$. The values $< cos(2\Delta\Phi) >$ (see Tab. 4) are obtained from the Monte Carlo simulation described in chapter 2.3. The simulation was tuned until the relevant experimental distributions (cf. Fig. 3) were matched which resulted in vanishing systematical errors of the correction factors (last column of Tab. 4). The corrected values P_2' are used to quantify the ratio R_N^{corr} of the number of particles emitted perpendicular to the number of particles emitted in the reaction plane: $R_N^{corr} = \{N(90°) + N(-90°)\}/\{N(0°) + N(180°)\} = \{1 - P_2'\}/\{1 + P_2'\}$. A ratio R_N^{corr} larger than unity implies a preferred out-of-plane emission. Figure 5 shows the ratio R_N^{corr} for
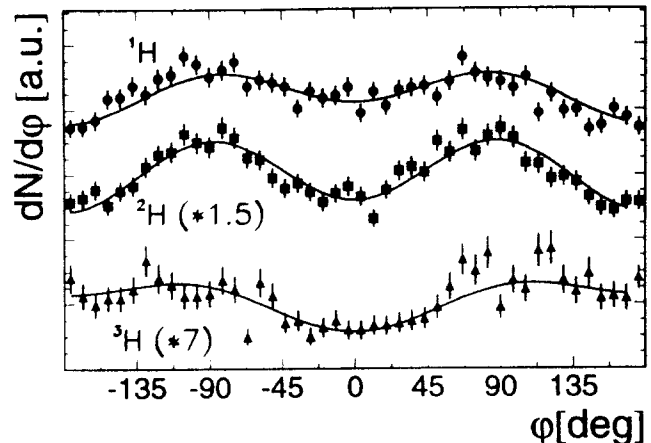

Fig. 4. Typical $dN/d\varphi$-distributions for H-isotopes measured at $E_{Lab}/A = 400$ MeV for semi-central collisions (MUL2,MUL3). The ordinate is linear starting at zero. The particles analysed stem from a momentum range of $400 < p_T/A < 500$ MeV/c. The solid lines are fits with $cos(\varphi)$ and $cos(2\varphi)$ terms.
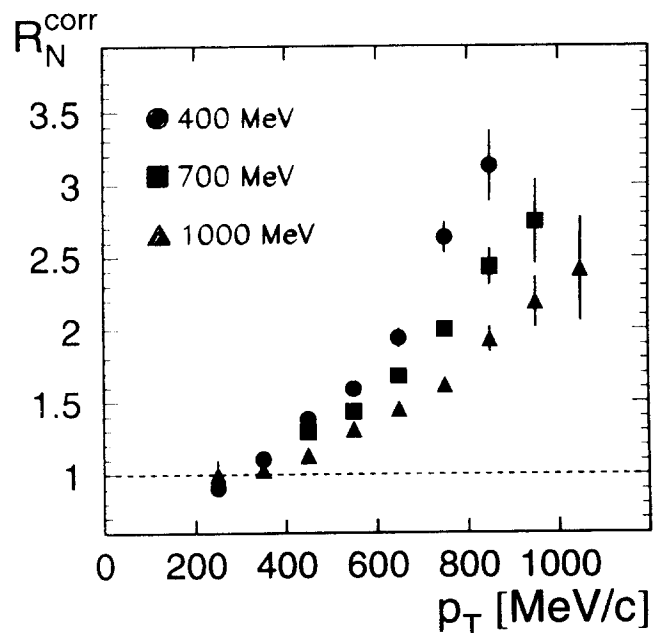

Fig. 5. The corrected out-of-plane/in-plane ratio R_N^{corr} for protons measured at $E_{Lab}/A = 400, 700$ and 1000 MeV. R_N^{corr} is shown as a function of the transverse momentum for semi-central collisions (MUL2,MUL3). The dashed line at $R_N^{corr} = 1$ indicates an isotropic emission at midrapidity.

protons as a function of the transverse momentum for different beam energies. The centrality cut corresponds to the sum of the multiplicity bins MUL2 and MUL3. The average impact parameter is estimated to be about $<b> \approx 7.5$ fm. A strong dependence of R_N^{corr} on the transverse momentum p_T is observed. The ratio increases with increasing p_T but decreases with increasing beam energy. The impact parameter dependence of R_N^{corr} is shown in Fig. 6 for three incident energies. The data indicate a strong dependence on the collision central-

ity. The strongest anisotropy is observed at the most peripheral collisions (MUL1). This observation is valid for $E_{Lab}/A = 700$ and 1000 MeV. In the case of MUL1 at 400 MeV the large reaction plane uncertainties (see Tab. 4) would cause relatively large errors on R_N^{corr}. Therefore, only the corresponding uncorrected parameter P_2 is given (Tab. 5).

p_T[GeV/c]	MUL1	MUL2	MUL3	MUL4
E_{Lab}/A = 400 MeV				
0.2-0.3	-0.04(1)	+0.01(1)	+0.03(1)	+0.04(1)
0.3-0.4	-0.03(1)	-0.05(1)	+0.00(1)	-0.01(1)
0.4-0.5	-0.03(1)	-0.07(1)	-0.06(1)	0.00(1)
0.5-0.6	-0.07(1)	-0.12(1)	0.07(1)	-0.02(1)
0.6-0.7	-0.11(2)	-0.15(1)	-0.11(1)	-0.03(1)
0.7-0.8	-0.09(2)	-0.21(1)	0.16(1)	-0.04(1)
0.8-0.9	-0.14(4)	-0.26(2)	0.18(3)	-0.04(1)
0.9-1.0	-0.17(9)	-0.35(4)	-0.22(5)	-0.06(2)
1.0-1.1	-0.04(19)	-0.38(8)	-0.22(11)	-0.08(3)
E_{Lab}/A = 700 MeV				
0.2-0.3	+0.04(15)	+0.21(13)	+0.01(12)	+0.04(10)
0.3-0.4	-0.06(2)	-0.06(1)	-0.05(1)	+0.01(1)
0.4-0.5	-0.08(1)	-0.09(1)	-0.04(1)	0.00(1)
0.5-0.6	-0.12(1)	-0.13(1)	-0.05(1)	0.00(1)
0.6-0.7	-0.15(1)	-0.17(1)	0.09(1)	0.00(1)
0.7-0.8	-0.18(2)	-0.21(1)	-0.13(1)	-0.01(1)
0.8-0.9	-0.21(3)	-0.29(2)	0.15(1)	0.04(1)
0.9-1.0	-0.27(6)	-0.30(4)	-0.19(2)	-0.03(2)
1.0-1.1	-0.22(12)	-0.24(7)	-0.29(4)	-0.03(3)
E_{Lab}/A = 1000 MeV				
0.2-0.3	-0.07(5)	-0.02(4)	+0.01(3)	+0.04(3)
0.3-0.4	-0.05(1)	-0.03(1)	+0.01(1)	+0.04(1)
0.4-0.5	-0.08(1)	-0.05(1)	-0.01(1)	+0.02(1)
0.5-0.6	-0.10(1)	-0.10(1)	-0.04(1)	+0.02(1)
0.6-0.7	-0.12(1)	-0.14(1)	-0.07(1)	+0.01(1)
0.7-0.8	-0.15(2)	-0.17(1)	-0.09(1)	0.00(1)
0.8-0.9	-0.18(3)	-0.22(2)	0.13(1)	-0.03(1)
0.9-1.0	-0.22(6)	-0.25(3)	-0.16(2)	0.00(2)
1.0-1.1	-0.23(11)	-0.27(6)	-0.18(4)	-0.02(2)

Table 5. Parameters P_2 not corrected for the reaction plane uncertainty for events in which protons were observed in the spectrometer in different p_T-intervals. The statistical errors are given in brackets. The values of MUL5 are comparable with zero within the error bars and therefore not shown

At $E_{Lab}/A = 400$ MeV not only protons but also composite particles have been measured. Table 6 shows the parameters P_2 for H- and He-isotopes for semi-central collisions (<b>≈7.5 fm). The correction factor for this centrality cut (MUL2, MUL3) is $<\cos(2\Delta\Phi)>=0.39$. A comparison of the H-isotopes shows a clear increase of the anisotropy with increasing mass of the fragment. Tritons and ^{3}He show the same anisotropy within the errors.
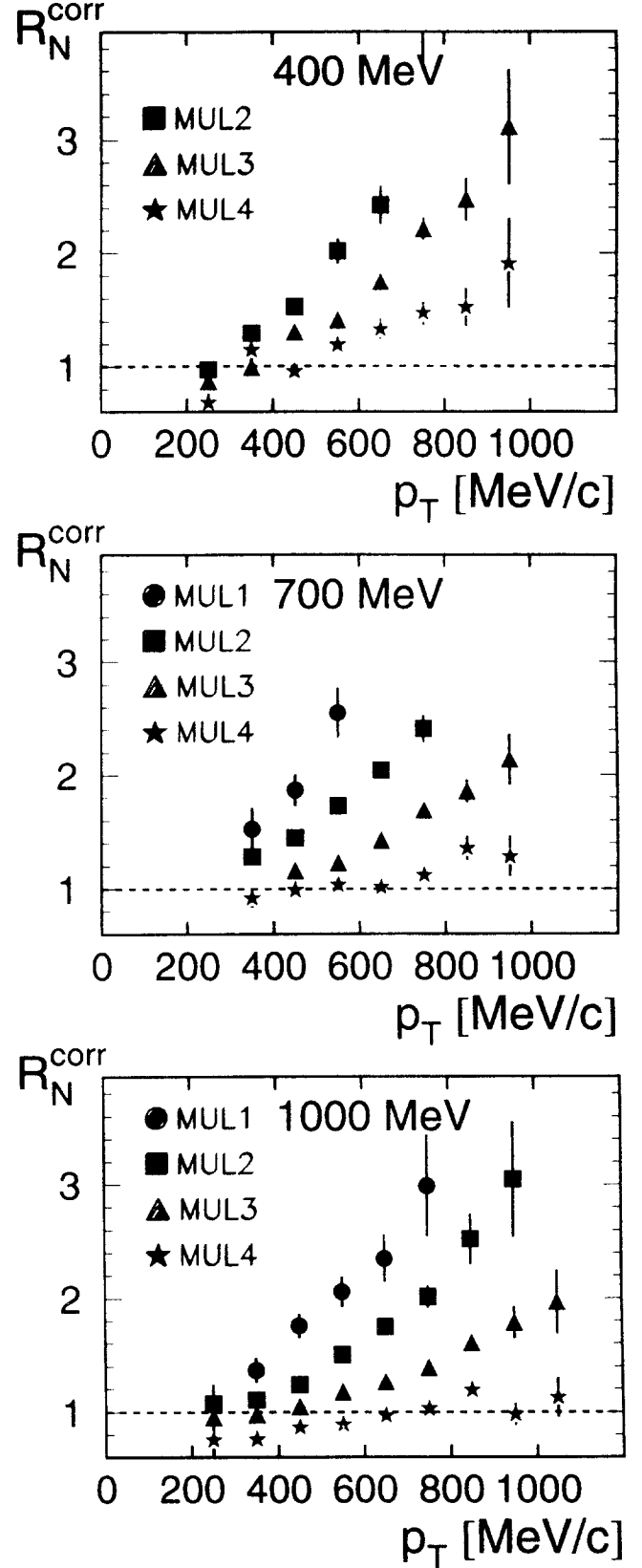

Fig. 6. The out-of-plane/in-plane ratio R_N^{corr} for protons measured at different incident energies E_{lab}/A. The R_N^{corr} is shown as a function of the transverse momentum for different multiplicity ranges. The values R_N^{corr} are corrected for the uncertainty in determining the reaction plane.

$E_{Lab}/A = 400$ MeV					
p_T/A	^{1}H	^{2}H	^{3}H	^{3}He	^{4}He
0.1-0.2	-	+0.04(2)	+0.01(3)	-	-0.03(4)
0.2-0.3	+0.02(1)	-0.01(1)	-0.06(1)	-0.07(2)	-0.13(1)
0.3-0.4	-0.02(1)	-0.08(1)	-0.15(1)	-0.13(1)	-0.16(1)
0.4-0.5	-0.06(1)	-0.15(1)	-0.22(4)	-0.24(1)	-0.25(2)
0.5-0.6	-0.09(1)	-0.21(1)		-0.29(3)	-0.34(6)
0.6-0.7	-0.12(1)	-0.27(3)	.	-0.33(7)	-0.58(19)
0.7-0.8	-0.18(1)	-			
0.8-0.9	-0.20(1)	-		.	.
0.9-1.0	-0.25(2)	-			
1.0-1.1	-0.26(4)	-			

Table 6. Parameters P_2 not corrected for the reaction plane uncertainty for different intervals p_T/A [GeV/c]. The values are given for semi-central collisions (MUL2, MUL3). The statistical errors are given in brackets.

4.1 Discussion

The energy dependence of the preferred emission out of plane is consistent with previous experiments. The Plastic-Ball collaboration found a maximum signal R_N for protons at a beam energy of $E_{Lab}/A = 400$ MeV and a decrease at higher incident energies [7]. Similar findings were reported by the LAND-collaboration for neutrons [9].

The impact parameter dependence shown in Fig. 6 is seemingly in disagreement to the Plastic-Ball data which show a maximum for semi-central collisions [7]. Our data indicate the strongest effect at the multiplicity bin MUL1 that corresponds to peripheral collisions. However, the Plastic-Ball data have not been corrected for uncertainties in determining the reaction plane. This reduces the values R_N for peripheral collisions since the uncertainties are larger than for semi-central collisions.

Moreover, the Plastic-Ball data are shown in the principal axis system of the tri-axial momentum ellipsoid. Due to sidewards flow into the reaction plane the orientation of this ellipsoid differs by the flow angle Θ_{flow} from the orientation of the beam axis. In peripheral collisions the flow is small but increases for decreasing impact parameter [23]. Large flow angles will lead to a lowering of R_N and R_N^{corr}, respectively, if evaluated relative to the beam axis. To get a quantitative understanding of such effects we have performed Monte Carlo simulations in a very simplified schematic model. The results of these are sketched in Fig. 7 in which an emission pattern is simulated that leads to similar ratios as measured at $E_{Lab}/A = 700$ MeV. The emission pattern is approximated by an ellipsoid in momentum space, whose shape and orientation is defined by the flow angle Θ_{flow} and two aspect ratios r_{31} and r_{21} [24]. The ellipses shown in Fig. 7 are contours of a Gaussian momentum distribution in the center-of-mass system. The axis r_2 of the ellipsoid coincides with the y-axis of the cm-coordinate system, whereas the axes r_1 and r_3 are rotated by Θ_{flow} versus the x- and z-axis, respectively. The reaction plane is denoted $p_x p_z$. It is obvious that the in-plane momentum component p_x is strongly affected by Θ_{flow}, whereas the out-of-plane component p_y does not change. Figure 8 shows the corresponding out-of-plane/in-plane ratios
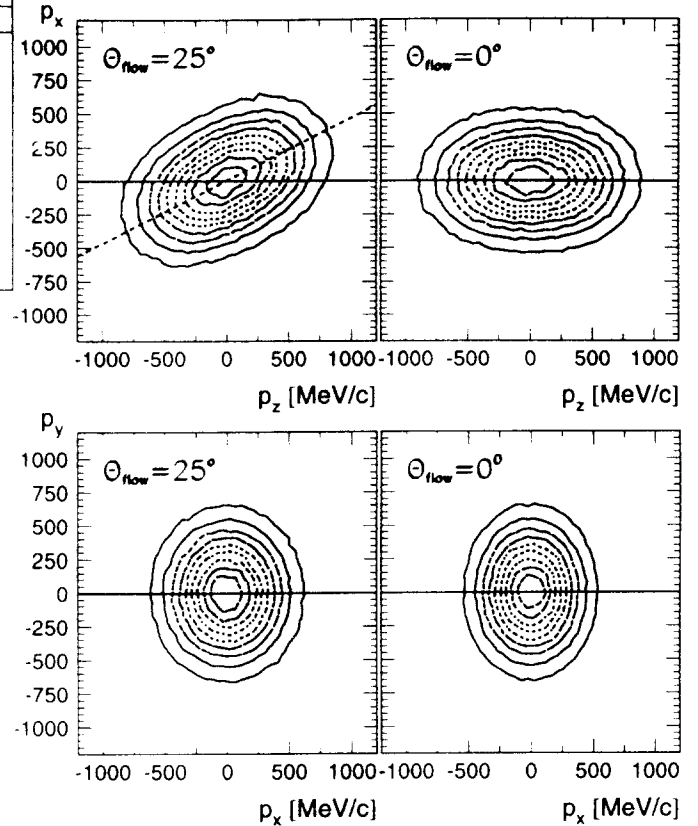

Fig. 7. Contours representing an anisotropic two-dimensional Gaussian momentum distribution obtained from a Monte Carlo simulation. Plotted are the in-plane aspect ratio $r_{31}=1.6$ (upper) and out-of-plane $r_{21}=1.3$(lower), respectively. On the right, the flow axis (dashed line) is rotated by the flow angle Θ_{flow}. The p_z-axis indicates the beam axis.
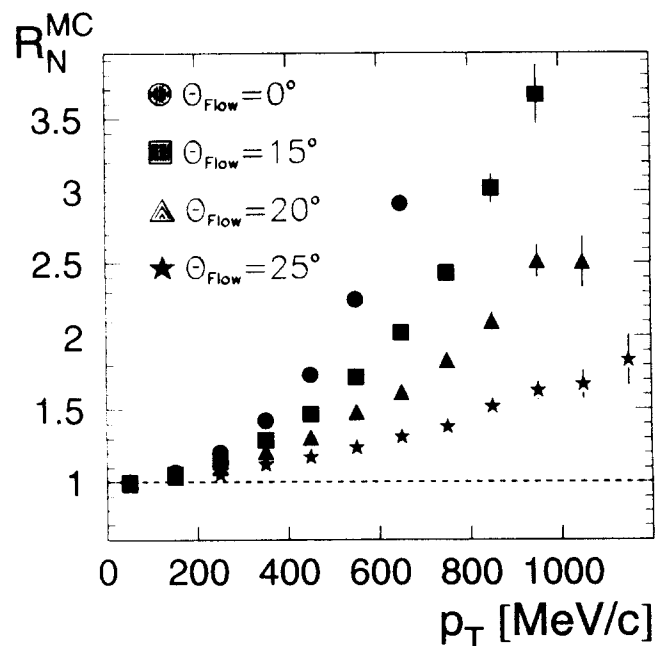

Fig. 8. Simulated out-of-plane/in-plane ratios R_N^{MC} with respect to the beam axis as function of p_T for different Θ_{flow}.

as a function of transverse momentum for different angles Θ_{flow} of the momentum ellipsoid with respect to the beam axis. $\Theta_{flow}=0^o$ means that the principal axis of the ellipsoid coincides with the beam direction. The figure demonstrates that the ratio R_N^{MC} is reduced in strength if Θ_{flow} is increased. The decreasing ratios of the measured data from MUL1 to MUL3 at $E_{Lab}/A = 700$ MeV (see Fig. 6) can be reproduced by changing the flow angle Θ_{flow} from 0 to 20 degrees. Therefore, the higher ratios R_N for peripheral (MUL1) compared to semi-central (MUL2, MUL3) collisions might be an artifact caused by higher Θ_{flow} in semi-central collisions. Even though the sidewards flow is larger in more central collisions (MUL4), the influence of Θ_{flow} on R_N is reduced due to a more isotropic configuration of the reaction geometry. Small flow angles are associated with elongated shapes $r_{31} > 1$, and larger flow angles with shapes closer to spherical symmetry ($r_{31} \approx 1$) [24]. In the limit of $r_{31} \rightarrow 1$ no influence of Θ_{flow} should be observed.

These considerations show that for an interpretation of the impact parameter dependence of the ratio R_N^{corr} around the beam axis the event shape has to be known. For a rotation of the momentum ellipsoid into the principal axis system the flow angle Θ_{flow} must be reconstructed on an event-by-event basis. This reconstruction can only be done by a sphericity analysis of 4π data. Since we observe only one particle per event in the spectrometer, our data can only be given with respect to the beam axis. It is worth noting that the determination of the true flow angle is a difficult experimental task even for 4π detectors since it is strongly affected by ever present acceptance limitations and the necessarily incomplete separation of spectator nucleons from participants.

In addition the above simulation shows that the increase of R_N^{MC} with increasing p_T can be generated by a phase space distribution based on Gaussian momentum sources assuming different widths for the p_x- and p_y-momentum distributions. This means that higher values of R_N at higher transverse momenta can be the trivial consequence of the corresponding phase space distribution. More sophisticated arguments predict that the azimuthal anisotropy vanishes quadratically with momentum as p_T tends to zero [25]. Nevertheless, compression effects of nuclear matter might influence the shape of the p_T-dependence. Indeed, recent studies in the framework of IQMD for neutrons have shown a sensitivity of R_N as a function of p_T to the EOS not only for data in the principal axis system but also for data taken around the beam axis. Our measured p_T-dependence is in qualitative agreement with microscopic model predictions [26].

A comparison of the azimuthal asymmetry observed in H-isotopes indicates an approximate linear increase of P_2 as a function of the fragment mass A (see Tab. 6). This is consistent with previous experiments which found that protons show a less pronounced effect than higher charged particles [7, 10]. This fact is related to a higher collectivity seen by composite particles, since single nucleons are more affected by thermal motion. ^{3}H and ^{3}He show the same anisotropy within the error bars. This
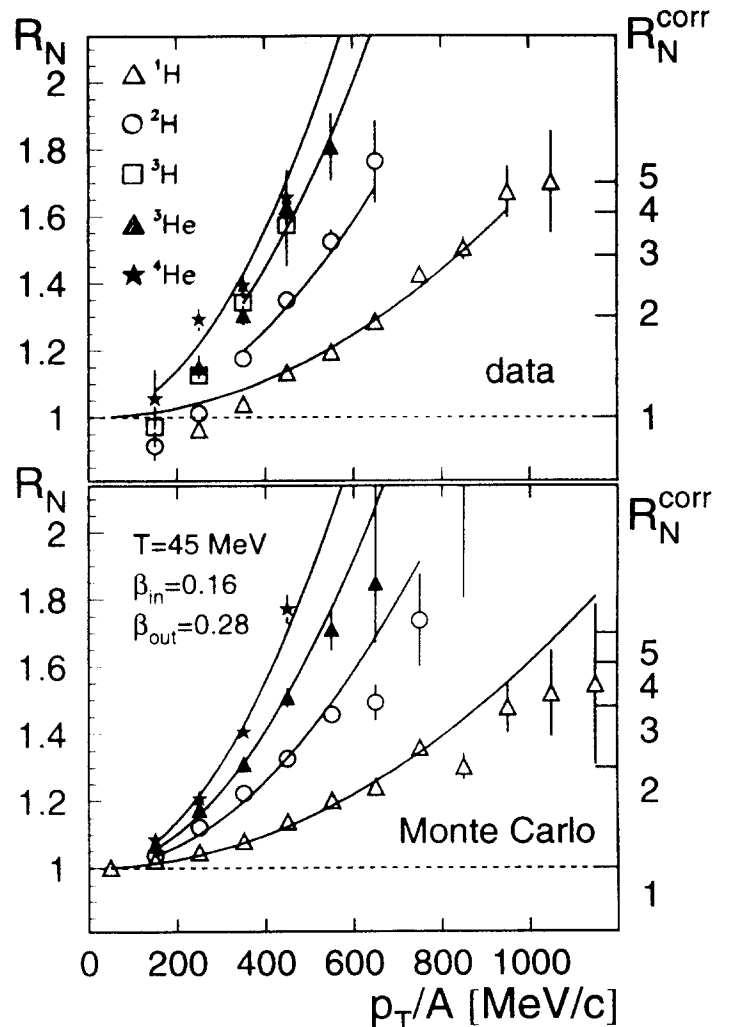

Fig. 9. The upper picture shows the measured out-of-plane/in-plane ratios R_N for different particles measured at $E_{Lab}/A = 400$ MeV. R_N is shown as a function of the transverse momentum divided by A for semi-central collisions (MUL2, MUL3). On the right ordinate the values corrected for s the reaction plane R_N^{corr} uncertainties are given. The lower picture shows calculated Monte Carlo ratios. The parametrization assumes a source temperature of T=45 MeV expanding with β_{in}=0.16, β_{out}=0.28 (lower). The ratios are parametrized by quadratic functions.

is clear evidence that Coulomb interactions do not affect the anisotropic emission out of the reaction plane, in accordance to what has been reported for protons and neutrons [9, 10].

4.2 Interpretation by a blast wave scenario

In the following we will discuss whether the experimental in-plane/out-of-plane ratios are in agreement with a blast wave scenario of nucleons at midrapidity in thermal equilibrium[27]. In this scenario a thermally equilibrated source of protons and composite particles with a temperature T is superimposed by a blast wave, characterized by a mean radial flow velocity β. The resulting momentum distribution is given by the expression [28]

$$\frac{d^3n}{dp^3} \sim e^{\frac{-\gamma E}{T}} [\frac{sinh\alpha}{\alpha})(\gamma E + T) - T cosh\alpha] \qquad (1)$$

where p is the momentum of the particle in the center of mass, $\gamma = (1-\beta^2)^{1/2}$, and $\alpha = \gamma\beta p/T$. In contrast to reference [28] we do not consider a spherically symmetric fireball expansion, but an asymmetric expansion with different radial flow velocities in-plane β_{in} and out-of-plane β_{out}. The aspect ratios r_{21}, r_{31} mentioned in chapter 4.1 can be interpreted as an anisotropic expansion with a higher mean radial flow velocity out-of-plane (y-axis) than in-plane (x-axis) and a higher longitudinal radial flow velocity along the z-axis than in-plane, respectively. The variation of the particle momenta resulting in $r_{21} > 1$ leads to a higher particle density $dN/d\varphi$ out-of-plane than in-plane. For the interpretation by a blast wave scenario we use the data measured at 400 MeV/A where we have the data of composite particles with their higher collectivity. At higher bombarding energies composite particles can not be measured at midrapidity because of the limited momentum acceptance of the spectrometer. In order to explore the parameters T, β_{in}, β_{out} describing the data, we compare the results of Monte Carlo calculations with the measured ratios in-plane/out-of-plane R_N. The parameters T, β_{in}, β_{out} fulfil the constraint that a fit with a Boltzmann formula without radial flow to the particle distribution would yield temperatures around $T_{Boltz} = 65$ MeV in accordance to previous experiments[30]. In the blast wave scenario we generated different event samples with source temperatures T of 40, 45 and 50 MeV common for all particle species. The values for β_{in} and β_{out} are chosen such that for the deuterons the simulated ratios agree best to the data. Following [25, 29] the calculations are done with a flow angle of $\Theta_{flow} = 20^o$. The longitudinal radial flow velocity along the p_z-axis (r_3) is assumed to be $\beta_{||} = 0.42$ which is the velocity of the projectile in the center of mass system at the beam energy of 400 MeV/A. This value leads to aspect ratios of approximately $r_{31} \approx 1.6$. In Fig. 9 the measured (upper) and simulated (lower) ratios are shown. To compare the measurement with the simulation the ratios are parametrized by quadratic functions $R_N(p_T) \sim 1 + a \cdot p_T^2$ [25]. The resulting fit parameter a as well as the χ^2 per degree of freedom are listed in Table 7. The best agreement is obtained by assuming a temperature around T=45 MeV and radial flow velocities in-plane of $\beta_{in} = 0.16$ and out-of-plane $\beta_{out} = 0.28$. As shown in chapter 4.1, the extracted values β_{in}, β_{out} depend on Θ_{flow} and r_{31}. Deviations from $\beta_{||} = 0.42$ by $\pm 20\%$ ($r_{31} \approx 1.6 \pm 10\%$) result in variations of $\pm 15\%$ in β_{out}.

Recent studies done by the EOS-collaboration for Au+Au collisions at $E_{Lab}/A = 400$ MeV yield similar results[31]. In these studies temperatures of approximately T=55 MeV and a collective radial flow velocity of $\beta_{radial} = 0.22$ were found. The value of T is somewhat higher than our results which can be explained by the fact that the EOS-group has analysed central events. This event class shows an isotropic emission pattern which therefore can be described by one common radial flow velocity β_{radial}.

Our calculation suggests that the data can be explained by a scenario assuming a source of protons and composite particles in thermal equilibrium. However, a detailed comparison of the data with the prediction of this schematic model reveals significant differences. The ratio R_N^{corr} as determined from the experimental data seems to rise only for p_T values above 200 MeV/c, whereas the model clearly predicts a rise already at $p_T = 0$. Apparently the data do not exhibit radial flow in the low momentum particles. The low p_T-isotropy may be an indication of different dynamics in this part of phase space.

	data		T=40 MeV β_{in}=0.19 β_{out}=0.30		T=45 MeV β_{in}=0.16 β_{out}=0.28		T=50 MeV β_{in}=0.11 β_{out}=0.26	
id	χ^2	a	χ^2	a	χ^2	a	χ^2	a
^{1}H	3.4	0.68(1)	3.3	0.66(1)	2.8	0.62(1)	0.9	0.53(1)
^{2}H	2.6	1.62(2)	0.8	1.63(1)	4.6	1.61(2)	3.2	1.60(2)
^{3}H	2.5	2.50(8)	1.0	2.39(2)	1.2	2.55(2)	3.4	2.66(2)
^{3}He	1.4	2.75(6)	-	-	-	-	-	-
^{4}He	1.6	3.47(9)	3.9	3.11(3)	2.5	3.47(3)	1.2	3.94(3)

Table 7. Parameters a of the function shown in Fig. 9. A fit assuming a purely thermal source without radial flow results in a source temperatures of T=65 MeV in each case.

5. Summary

In summary, we have studied the beam energy and impact parameter dependence of so-called squeeze-out effects for the system ^{209}Bi+^{209}Bi at projectile energies of $E_{lab}/A = 400$, 700, and 1000 MeV. For the first time particle ratios out-of-plane/in-plane corrected for uncertainties in determining the reaction plane are presented. We observe an enhanced emission of particles perpendicular to the reaction plane. Composite particles exhibit a more pronounced out-of-plane emission: The magnitude of the out-of-plane parameter P_2 is proportional to the mass of the particles. Coulomb interactions do not affect the anisotropic emission perpendicular to the reaction plane. The anisotropy is seemingly most pronounced for peripheral collisions and decreases with increasing beam energy. For an interpretation of the magnitude of the out-of-plane/in-plane ratio collective sidewards flow effects have to be taken into account. The experimental data available so far do not allow an unambiguous separation of directed flow and squeeze effects. The increasing p_T-dependence of the ratio R_N seems to be the result of decompression expansion effects; it reflects the resulting characteristic phase space distribution of the ejected matter. Finer details of the influence of decompression effects on the p_T-dependence of R_N can be extracted only from microscopic model calculations. Their comparison with experimental data is expected to lead to an improved determination of the EOS. For a comparison of the squeeze-out signal shown around the beam axis the models must reproduce the shape of the momentum ellipsoid as well as the sidewards flow correctly.

Acknowledgement

References

1. R. Stock, Phys. Rep. 135, 259(1986).

2. H. Stöcker and W. Greiner, Phys. Rep. 137, 277(1986).

3. W. Cassing, V. Metag, U. Mosel and K. Niita, Phys. Rep. 188, 365(1986).

4. H. H. Gutbrod, K. H. Kampert, B. W. Kolb, A. M. Poskanzer, H. G. Ritter, H. R. Schmidt, Phys. Lett 216B, 267(1989).

5. M. Demoulins, D. L'Hote, J. P. Alard, J. Augerat, R. Babinet, N. Bastid, F. Brochard, C. Cavata, N. De Marco, P. Dupieux, H. Fanet, Z. Fodor, L. Fraysse, P. Gorodetzky, J. Gosset, T. Hayashino, M. C. Lemaire, A. Le Merdy, B. Lucas, J. Marroncle, G. Montarou, M. J.Parizet, J. Poitou, C. Racca, W. Schimmerling, Y. Terrien and O. Valette, Phys. Lett. B241, 476(1990).

6. J. Gosset, M. Demoulins, R. Babinet, C. Cavata, H. Fanet, D. L'Hote, B. Lucas, J. Poitou, M. C. Lemaire, J. P. Alard, J. Augerat, N. Bastid, P. Charmensat, P. Dupieux, L. Fraysse, J. Marroncle, G. Montarou, M. J Parizet, D. Qassoud, A. Rahmani, F. Brochard, P. Gorodetzky and C. Racca, Phys. Lett. B247, 233(1990).

7. H. H. Gutbrod, K. H. Kampert, B. W. Kolb, A. M. Poskanzer, H. G. Ritter, R. Schicker, H. R. Schmidt, Phys. Rev. C42, 640(1990).

8. Y. Leifels, T. Blaich, T. W. Elze, H. Emling, H. Freiesleben, K. Grimm, W. Henning, R. Holzmann, J. G. Keller, H. Klingler, J. V. Kratz, R. Kulessa, D. Lambrecht, S. Lange, E. Lubkiewicz, E. F. Moore, W. Prokopowicz, R. Schmidt, C. Schütter, H. Spies, K. Stelzer, J. Stroth, E. Wajda, W. Walus, M. Zinser, E. Zude, and the FOPI Collaboration, Phys. Rev. Lett. 71, 963(1993)

9. D. Lambrecht, T. Blaich, W. Elze, H. Emling, H. Freiesleben, K. Grimm, W. Henning, R. Holzmann, J. G. Keller, H. Klingler, J. V. Kratz, R. Kulessa, S. Lange, Y. Leifels, E. Lubkiewicz, E. F. Moore, W. Prokopowicz, R. Schmidt, C. Schütter, H. Spies, K. Stelzer, J. Stroth, E. Wajda, W. Walus, M. Zinser, E. Zude, and the FOPI Collaboration, Z. Phys. A350, 115(1994).

10. A. Kugler, V. Wagner, M. Pachr, M. Sumbera, Yu. G. Sobolev, S. Hlavác, R. S. Simon, R. Lorencz, R. Wohlgemuth, Phys. Lett. B, 319(1994).

11. H. Stöcker, L. P. Csernai, G. Graebner, G. Buchwald, H. Kruse, R. Y. Cusson, J. A. Maruhn and W.Greiner, Phys. Rev. Lett. 52, 1594(1982)

12. Ch. Hartnack, M. Berenguer, A. Jahns, A. v. Keitz, R. Mattiello, A. Rosenhauer, J. Schaffner, Th. Schönfeld, H. Sorge, L. Winkelmann, H. Stöcker and W. Greiner, Nucl. Phys. A538, 53c(1992).

13. G. Welke, M. Prakash, T. T. S. Kuo, S. Das Gupta and C. Gale, Phys. Rev. C38, 2101(1988).

14. C. Hartnack, J. Aichelin, H. Stöcker, W. Greiner, Phys. Lett. B336, 131(1994).

15. P. Senger, W. Ahner, P. Baltes, P. Beckerle, C. Bormann, D. Brill, M. Cieślak, E. Grosse, W. Henning, P. Koczoń, B. Kohlmeyer, W. Konrad, D. Miśkowiec, C. Müntz, H. Oeschler, H. Pöppl, W. Prokopowiecz, F. Pühlhofer, S. Sartorius, R. Schicker, B. Schlei, E. Schwab, Y. Shin, J. Speer, J. Stein, K. Stiebing, R. Stock, H. Ströbele, C. Sturm, K. Völkel, A. Wagner, W. Waluś, Nucl. Instr. Meth. A 327, 393(1993).

16. W. Ahner, P. Baltes, C. Bormann, D. Brill, R. Brockmann, M. Cieślak, E. Grosse, W. Henning, P. Koczoń, B. Kohlmeyer, W. Konrad, D. Miśkowiec, C. Müntz, H. Oeschler, H. Pöppl, W. Prokopowicz, F. Pühlhofer, R. Renfordt, A. Sandoval, S. Sartorius, R. Schicker, E. Schwab, P. Senger, Y. Shin, J. Stein, K. Stiebing, R. Stock, H. Ströbele, K. Völkel, A. Wagner, W. Waluś, Z. Phys. A 341, 123(1991).

17. D. Brill, W. Ahner, P. Baltes, R. Barth, C. Bormann, M. Cieślak, M. Dębowski, E. Grosse, W. Henning, P. Koczoń, B. Kohlmeyer, D. Miśkowiec, C. Müntz, H. Oeschler, H. Pöppl, F. Pühlhofer, S. Sartorius, R. Schicker, P. Senger, Y. Shin, J. Speer, J. Stein, K. Stiebing, R. Stock, H. Ströbele, K. Völkel, A. Wagner, W. Waluś, Phys. Rev. Lett. 71, 336(1993).

18. D. Miśkowiec, W. Ahner, R. Barth, M. Cieślak, M. Dębowski, E. Grosse, W. Henning, P. Koczoń, R. Schicker, E. Schwab, P. Senger, P. Baltes, C. Müntz, H. Oeschler, S. Sartorius, C. Sturm, A. Wagner, P. Beckerle, C. Bormann, D. Brill, Y. Shin, J. Stein, R. Stock, H. Ströbele, B. Kohlmeyer, H. Pöppl, F. Pühlhofer, J. Speer, K. Völkel, W. Waluś, Phys. Rev. Lett. 72, 3650(1994).

19. J. Gosset, H. H. Gutbrod, W. G. Meyer, A. M. Poskanzer, A. Sandoval, R. Stock and G. D. Westfall, Phys. Rev. C16, 629(1977).

20. J. Speer et al., (to be published).

21. D. Brill, PhD Thesis, Universität Frankfurt/M.(1993), GSI report 93-36 (ISSN 0171-4546)

22. P. Danielewicz and G. Odyniec, Phys. Lett. 157B, 147(1985).

23. H. A. Gustafsson, H. H. Gutbrod, B. Kolb, H. Löhner, B. Ludewigt, A. M. Poskanzer, T. Renner, H. Riedesel, H. G. Ritter, A. Warwick, F. Weik, and H. Wieman, Phys. Rev. Lett. 52, 1590(1984).

24. P. Danielewicz, H. Ströbele, G. Odyniec, D. Bangert, R. Bock, R. Brockmann, J. W. Harris, H. G. Pugh, W. Rauch, R. E. Renfordt, A. Sandoval, D. Schall, L.S. Schroeder, and R. Stock, Phys. Rev. C38, 38(1988).

25. P. Danielewicz, Phys. Rev. C51, 716(1995).

26. S. A. Bass, C. Hartnack, H. Stöcker, W. Greiner, Z. Phys. A352, 171(1995).

27. J. P. Bondorf, S. I. A. Garpman, and J. Zimanyi, Nucl. Phys. A296, 320(1978).

28. P. J. Siemens and J. O. Rasmussen, Phys. Rev. Lett. 42, 880(1979).

29. Proceedings of a NATO Advanced Study Institute on The Nuclear Equation of State, Peniscola, Spain, NATO ASI Series B: Physics 216B(1989).

30. K. H. Kampert, in Proceedings of the International Workshop on Gross Properties of Nuclei and Nuclear Excitation XVI, Hirschegg, Austria, 1988, edited by H. Feldmeier (GSI, ISSN 0720-8715,Darmstadt, Germany, 1988).

31. M. A. Lisa, S. Albergo, F. Bieser, F. P. Brady, Z. Caccia, D. A. Cebra, A. D. Chacon, J. L. Chance, Y. Choi, S. Costa, J. B. Elliott, M. L. Gilkes, J. A. Hauger, A. S. Hirsch, E. L. Hjort, A. Insolia, M.Justice, D. Keane, J. Kintner, H. S. Matis, M. McMahan, C. McParland, D. L. Olson, M. D. Partlan, N. T. Porile, R. Potenza, G. Rai, J. Rasmussen, H. G. Ritter, J. Romanski, J. L. Romero, G. V. Russo, R. Scharenberg, A. Scott, Y. Shao, B. K. Srivastava, T. J. M. Symons, M. Tincknell, C. Tuvé, S. Wang, P. Warren, G. D. Westfall, H. H. Wieman, and K. Wolf (EOS-collaboration), Phys. Rev. Lett. 75, 2664(1995).